AIAA 2002-3041

Spontaneous Raman Scattering Diagnostics for High-Pressure Gaseous Flames

J. Kojima and Q. V. Nguyen

NASA Glenn Research Center
Cleveland, OH

22nd AIAA Aerodynamic Measurement Technology and Ground Testing Conference
24-27 June, 2002 / St. Louis, MO

Spontaneous Raman Scattering Diagnostics for High-Pressure Gaseous Flames

Jun Kojima[§] and Quang-Viet Nguyen[¶]

NASA Glenn Research Center, Cleveland OH 44135

Abstract

A high-pressure (up to 60 atm) gaseous burner facility with optical access that provides steady, reproducible flames with high precision, and the ability to use multiple fuel/oxidizer combinations has been developed. In addition, a high-performance spontaneous Raman scattering system for use in the above facility has also been developed. Together, the two systems will be used to acquire and establish a comprehensive Raman scattering spectral database for use as a quantitative high-pressure calibration of single-shot Raman scattering measurements in high-pressure combustion systems. Using these facilities, the Raman spectra of H_2-Air flames were successfully measured at pressures up to 20 atm. The spectra demonstrated clear rotational and ro-vibrational Raman features of H_2, N_2, and H_2O. The theoretical Raman spectra of pure rotational H_2, vibrational H_2, and vibrational N_2 were calculated using a classical harmonic-oscillator model with pressure broadening effects and fitted to the data. At a gas temperature of 1889 K for a $\phi = 1.34$ H_2-Air flame, the model and the data showed good agreement, confirming a ro-vibrational equilibrium temperature.

1. Introduction

Many qualitative measurements of species concentration and/or temperature by laser-based diagnostics have been performed in combustion environments over the past 20 years, but what is still critically needed for the validation of computational models used to design low-emission aircraft engines is 'quantitative' single-shot information of species and temperature at high pressures. Especially with the rapid development of the new generation of ultra-high pressure ratio gas turbine engines (> 30 atm), quantitative code validation data in high-pressure environments will become increasingly more in demand. Spontaneous laser Raman scattering (SRS) spectroscopy has been widely recognized as one of the few quantitative technique that provides spatially and temporally resolved simultaneous multi-species concentrations for major combustion products (N_2, O_2, CO_2, H_2, CO, H_2, CH_4, etc) and temperature [1, 2]. SRS measurements are relatively simpler, less expensive, and more versatile to obtain quantitative data than coherent anti-Stokes Raman spectroscopy (CARS) or stimulated Raman spectroscopy [1]. Another advantage of SRS for practical industrial applications is its ability to work with a single port if the back-scattered Raman signal is collected [3, 4, 5]. One can expect high quality SRS data with good signal-to-noise ratio (SNR) using either a UV-Raman technique [2, 6-10] or with a modified visible-Raman technique including high-energy longer pulse [11-13] and a non-intensified CCD with a mechanical gate [14-16]. The limitation of SRS is its relatively lower intensity and disturbances by background emissions. Detailed parametric discussion about SRS measurements based on SNR in both a UV-Raman system and a Nd:YAG-based system has been made by Miles [14]. Moreover, Raman scattering signal in high-pressure environments should be stronger than that at atmospheric pressure because it scales linearly with the number density of molecules.

A number of SRS measurements in high-pressure environments such as gas turbine combustors [13] or internal combustion engines [14, 17] have been made in terms of species concentrations but there are few works that include the quantitative pressure dependence effects of SRS on combustion species. Gu, et al., concluded, based on their non-combusting Raman-cell measurements, that SRS signals are a linear function of gas density and provide a quantitative measurement of density, and that the temperature can be determined even in high-pressure region around 60 bar after a calibration is made for a given experimental setup [18]. The known room-temperature cross-sections of the molecules and the spectrally integrated peak area for each Raman band are typically used to calibrate Raman scattering intensity to the molecular density. However, this calibration for accurate quantitative numbers *is* a challenge in practical high-pressure and -temperature flames because there are a lot of spectral interferences against pure Raman spectra that need to be accounted in for the corrections [7, 11, 14]. Furthermore, it is likely that pressure dependence on the spectral shape of the

[§] NRC Research Associate: MS OAI, 22800 Cedar Point Rd., Cleveland, OH 44142, Phone: (440) 962-3095, Email: Jun.Kojima@grc.nasan.gov

[¶] Aerospace Engineer: MS 5-10, Cleveland, OH 44135, Phone: (440) 433-3574, Email: Quang-Viet.Nguyen@grc.nasa.gov

Raman band by molecular collisions influences such interferences and also changes the so-called *band factors* [1] especially at high-temperatures. That is why a comprehensive Raman spectra database of high-pressure flames is still required for a quantitatively precise analysis in high-pressure combustion environments.

High-density gases in high-pressure cells [18] are typically used to study pressure dependence of Raman spectra but real combustion experiments are preferable to look at the spectral interferences in details. A number of Raman scattering measurements have been carried out in high-pressure combustors [13] or internal combustion engines [14]. However, such facilities are not suitable for collecting a Raman spectra database at high-pressure conditions because it is difficult to provide stable, repeatable, and a reliable source of combustion products for the purpose of acquiring a precise calibration standard.

The goal of our research is to investigate the entire Raman spectra for truly quantitative, multi-species information of molecular density and temperature in high-pressure combustion environments. In the present work we measured the high-pressure Raman spectra of the major combustion species in the precisely controlled gas burner that generate stable H_2/air flames at elevated pressures from 2 to 20 atm using high-performance spontaneous Raman diagnostics. The theoretical spectra of pure rotational H_2 Raman, vibrational H_2 Raman, and vibrational N_2 calculated using a classical harmonic-oscillator model and a line-shape model including pressure-broadening effects were compared to the experimental data to estimate the temperature.

2. Theoretical Modeling of Raman Spectra

2-1. Raman Cross-Sections

The theory of Raman scattering in diatomic and polyatomic molecules is well established [19]. According to Placzek's polarization theory of the Raman effect, the corresponding differential Raman scattering cross-section per molecule at thermal equilibrium is given by [19]

$$\left(\frac{\partial\sigma}{\partial\Omega}\right)^{\theta}_{i\to f} = \left(\frac{\pi}{\varepsilon_0}\right)^2 (\nu_0 \pm \nu_k)^4 g_i \frac{\exp(-E_i/kT)}{Q(T)} \Phi(a^2, \gamma^2, \theta) \tag{1}$$

Here, the superscript θ indicates the relative angle of the planes of polarization between scattered and incident light; the subscripts of i and f stand for the initial and final states respectively; ε_0 is the vacuum permittivity; ν_0 is incident light (laser) frequency; + and − signs refer to anti-Stokes and Stokes Raman scattering respectively; ν_k is molecular vibrational frequency associated with the rotation-vibration transition from i to f; g_i is the total degeneracy; E_i is the energy of the initial state; k is the Boltzmann constant; T is the gas temperature; $Q(T)$ is the total partition function of the molecule at temperature T; $\Phi(a^2, \gamma^2, \theta)$ is a function of the mean value of the derived polarizability tensor a^2, the anisotropy γ^2, and θ is the observation angle that stands for the molecule-dependent temperature-independent invariant, which is tabulated by Long [19] for every branch of ro-vibration and pure rotation scatterings. Note that the factors $(v+1)b_v^2$ and vb_v^2 should be multiplied to Eq. (1) for ro-vibration Stokes and anti-Stokes scattering of diatomic molecule respectively, here v is the vibrational quantum number and b_v^2 is defined as $h/8\pi^2 c\nu_k$ where h is the Plank constant, c is the speed of light. The Raman spectral line locations, given by molecule vibrational frequency ν_k, are calculated on the basis of energy conservation as

$$\nu_k = \frac{E_f - E_i}{hc} \tag{2}$$

where E_f is the energy of the final state. The energy in a vibrational-rotational state (v, J) is expressed as the sum of the vibrational energy term, $G(v)$ and rotational energy term, $F(v,J)$

$$E(v,J) = \frac{G(v) + F(v,J)}{hc} \tag{3}$$

According to the anharmonic oscillator model, $G(v)$ of diatomic molecules may be given by [20]

$$G(v) = \omega_e\left(v+\frac{1}{2}\right) - \omega_e x_e\left(v+\frac{1}{2}\right)^2 + \omega_e y_e\left(v+\frac{1}{2}\right)^3 \tag{4}$$

here ω_e, $\omega_e x_e$, and $\omega_e y_e$ are molecular constants and tabulated by Hertzberg [21]. According to the non-rigid rotator model that takes the influence of centrifugal force due to vibration into account, the rotational term for the *singlet* $^1\Sigma$ state of diatomic molecules such as N_2 or H_2 may be given by

$$F(v,J) = B_v J(J+1) - D_v J^2 (J+1)^2 \tag{5}$$

where $B_v = B_e - \alpha_e(v + 1/2)$, and $D_v = D_e + \beta_e(v + 1/2)$ where B_e, D_e, α_e, and β_e are molecular constants, which

are tabulated by Hertzberg [21]. Thus for a Stokes Q-branch, that is $\Delta v = v_f - v_i = +1$ and $\Delta J = J_f - J_i = 0$, Raman line frequency is given by

$$v_k(v,J) = \frac{E(v_i+1) - E(v_i)}{hc} \tag{6}$$

It should be noted that Q-branch of ro-vibrational Raman line is much stronger than the O- and S-branch because the polarizability tensor greatly exceeds the anisotropy invariant. So we calculate only Q-branch of ro-vibrational Raman scattering for diatomic molecule in the present model.

For S-branch (Stokes) of H_2 rotational Raman, the function $\Phi(a^2, \gamma^2, \theta)$ is proportional to the anisotropy, γ^2, and the following Placzek-Teller coefficients [19]

$$b_{J+2,J} = \frac{3(J+1)(J+2)}{2(2J+1)(2J+3)} \tag{7}$$

Also, $E(J) = F(J)/hc$ in Eq.(3) where $F(J) = B_e J(J+1) - D_e J^2(J+1)^2$, $v_k = E(J_i+2) - E(J_i)$ in Eq.(6), and $Q(T) = Q_{rot}$ in Eq.(7) should be replaced.

Thus, Raman line frequencies and cross-sections of ro-vibrational H_2 and pure rotational H_2 were calculated using above expressions. Note that we calculated the *relative* (but quantitative) intensity instead of absolute number by setting the function Φ and molecular-independent constants as a constant number so that the calculated Raman intensity can be fitted to experimental data of each molecule individually to determine temperature.

2-2. Line-Shape

A spectral profile of the Raman spectrum at atmospheric pressure is typically modeled using Gaussian profiles but those at high-pressure should be described by line-shape models that includes collisional-broadening effects. The Voigt function, which is the convolution of the Gaussian and Lorentz distributions, is usually used as a better way to model such a spectrum. Here we used a Voigt function [22] for Raman spectra modeling although even Voigt profiles may not be valid in the far wings of line shapes at high-pressure due to break down of the impact approximation [23].

Voigt-*a* and -*x* parameter are given by

$$a(v,J,P,T) = \sqrt{\ln 2}\,\frac{\Delta\nu_C(P,T)}{\Delta\nu_G(v,J)} \tag{8}$$

$$x(v,J) = 2\sqrt{\ln 2}\,\frac{(v - v_k(v,J))}{\Delta\nu_G(v,J)} \tag{9}$$

where $\Delta\nu_G$ is the overall convolution Gaussian width [cm^{-1}] and may be written as

$$\Delta\nu_G(v,J) = \sqrt{(\Delta\nu_D^{\,2} + \Delta\nu_{Laser}^{\,2} + \Delta\nu_{Spec}^{\,2})} \tag{10}$$

where $\Delta\nu_D$ is the molecular-dependent Doppler width [cm^{-1}], $\Delta\nu_{Laser}$ is the injection-seeded laser line width, 0.003 [cm^{-1}], and $\Delta\nu_{Spec}$ is the spectral resolution of the spectrograph, 14.0 [cm^{-1}] as a instrumental function. $\Delta\nu_C$ is the collisional broadening width [cm^{-1}] and $\Delta\nu_C = 2\gamma(P,T)$, where $\gamma(P,T)$ is the pressure broadened line halfwidth (HWHM) [cm^{-1}/atm] for a gas total pressure P [atm], temperature T [K], and partial pressure of the molecule P_s [atm]. It is given by [24]

$$\gamma(P,T) = \left(\frac{T_0}{T}\right)^n \left[\gamma_{air}(P_0,T_0)(P - P_s) + \gamma_{self}(P_0,T_0)P_s\right] \tag{11}$$

where $\gamma_{air}(P_0,T_0)$, and $\gamma_{self}(P_0,T_0)$ are air-broadened, and self-broadened width at 296 K and 1 atm. n is the coefficient of temperature dependence of air-broadened halfwidth and here the classical value of 0.5 [24] was used for all cases. $\gamma_{air}(P_0,T_0)$, and $\gamma_{self}(P_0,T_0)$ for all N_2 Raman lines over the range of combustion temperature were assumed to the same value of 0.048 [cm^{-1}/atm] that was derived from HITRAN96 [24] by calculating an *intensity-weighted* average halfwidth of absorption Q-branch lines from J = 1 to 40 in the (1,0) vibrational transition which is the dominant transition at room temperature. We used one fixed number for all pressure broadened linewidths even though they are transition dependent, because those for "hot" lines are not well known. As for H_2, unfortunately, detailed line information about pressure broadening has not been available in the literatures, so we assumed 0.05 cm^{-1} as a typical width [24]. Note that when $\Delta\nu_{Spec} >> \Delta\nu_C$, Voigt-a becomes nearly zero, so a Voigt profile becomes a Gaussian profile. In the present experiment $\Delta\nu_{Spec}$ is a dominant factor for $\Delta\nu_G$ because $\Delta\nu_{Spec} >> \Delta\nu_D >> \Delta\nu_{Laser}$.

Finally, the profile of Raman spectra at the temperature (T) and pressure (P) of interest were calculated by integration (sum) of all Voigt lines based on the assumption of the additive approximation. It should be noted that the interaction between different transitions, the so-called line-mixing [25] in Raman spectra of high-pressure gases, was not included in the present model. Fortunately, line-narrowing and line-shift of N_2 Raman due to such line-mixing effects over the range of pressure up to 60 atm have been observed by an order of 10^{-1} cm^{-1} [26], so these effects may not be

significant compared to the spectral resolution of the present Raman measurement.

3. Experimental Apparatus

3-1. High-Pressure Burner

A specially designed high-pressure gaseous burner was used to provide a controllable and stable source of combustion products in high-pressure environments for the calibration and development of the quantitative Raman diagnostic technique. Figure 1 shows the assembly diagram of the burner nozzle which consists of a staggered (alternating) micro-tube array, in which an 8 x 8 array of 1.1 mm diameter holes spaced at 2.6 x 2.6 mm are fed by an oxidizer cavity located just underneath the burner surface. Additionally, a 7 x 7 array of 1.1 mm diameter holes located between oxidizer holes are fed by a fuel cavity. Rapid mixing of fuel and oxidizer is enhanced by micro-jets at high velocity from the tubes which permits the operation of non-premixed flame to behave as a quasi-premixed flame. The burner produces a region of combustion products directly downstream of the flame with a uniform flow pattern over an approximate 5 x 5 mm zone. The thick 300 series stainless steel burner face is

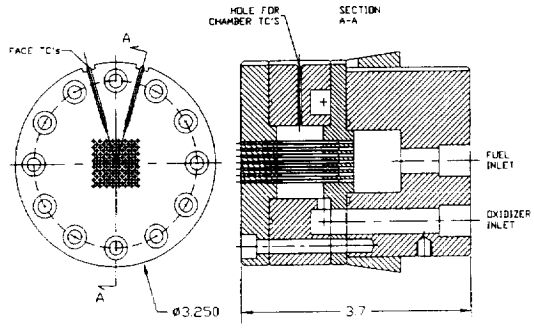

Fig. 1 Micro-tube non-premixed burner nozzle. Dimensions are in inches.

convectively cooled by both the flow of the ambient temperature air and fuel, and by the conduction of the main burner body. Note that a non-premixed flame featured by multiple mm-order holes can keep the burner surface far below 400 °C preventing meltdown at high-pressure and high-temperature combustion.

Figure 2 shows a schematic of the high-pressure burner rig and gas flow system. Room-temperature air from a facility compressor provided 30 atm air for cooling. The cooling air is introduced at the bottom of

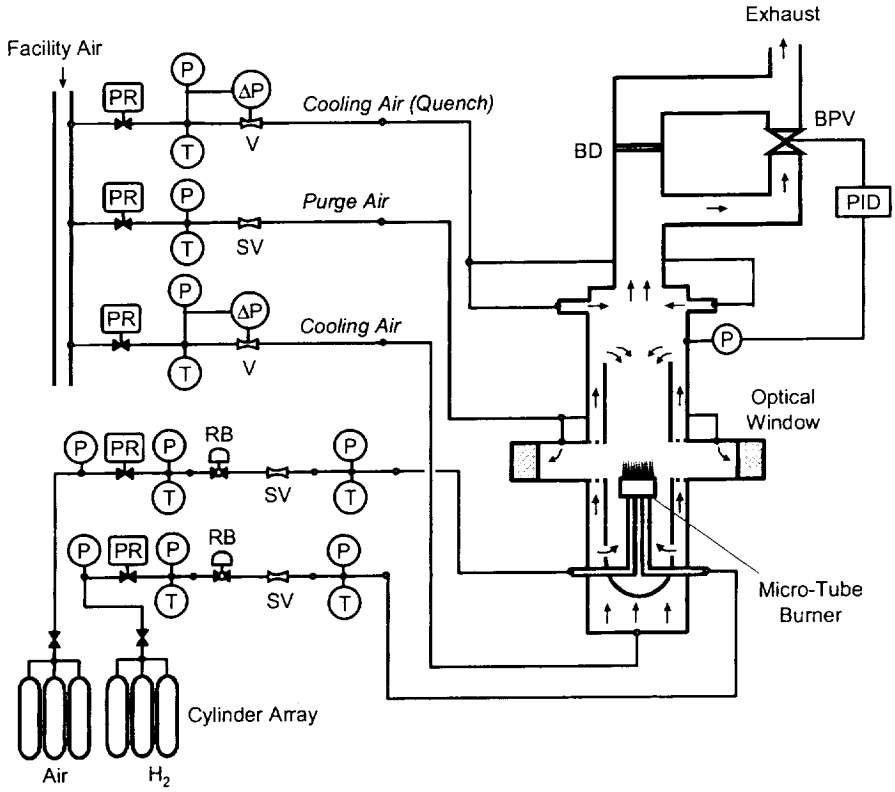

Fig. 2 High-pressure gaseous burner rig and gas flow system. P: Pressure Transducer; T: Thermocouple; PR: Remotely Operated Regulator; RB: Remotely Operated Ball Valve; V: Venturi; SV: Sonic Venturi; BPV: Back-Pressure Valve; PID: Process Controller; BD: Burst Disk

the rig for liner cooling (0.25 lbm/s max.), and also at the upper side as "quenching" (0.20 lbm/s max.). These airflows were controlled by remotely operated regulators using calibrated venturi flow meters. Approximately 10 % or less of the total cooling flow rate of the facility air was used as a purge-air for the optical windows during experiments prevent water vapor condensation. The flow rate of the purge-air was set via the sonic venturi. The pressure of the burner rig was maintained via the back-pressure valve mounted at the top of the chamber, which is remotely operated by auto-feedback process controller. The burner rig was operated at 20 atm in the present study while rig pressure can range from 1 atm to 60 atm. The pressure was stabilized below ± 1 % for each condition. For optical access, the burner rig has four 44 mm thick UV grade fused silica windows with a clear aperture of 85 mm. A burst disk (935 psig) placed between the pressure chamber and exhaust pipe is required in case of a hazardous pressure buildup or an unexpected explosion.

The micro-tube burner is mounted inside the high-temperature liner casing inside the rig. Note that the pressure inside the casing is the same as for the rig. A small amount of cooling bleed air is fed into the casing to avoid building up of combustion products around the burner. The oxidizer air and the fuel H_2 were provided by 12-pack cylinder arrays at 150 atm pressure. The flow rates of the air and fuel were precisely controlled within 1 % accuracy using the sonic venturi flow meters with computer operated regulators and valves. For the data presented in this paper, the equivalence ratio was set at $\phi = 1.34$ while it can be operated over a wide range from $\phi = 0.3$ to 4.

Measurements were made at 25 mm above the burner nozzle surface on the center axis. This is a point located approximately just above the actual flame zone.

3-2. Raman Diagnostics

Figure 3 shows a schematic of Raman scattering measurements apparatus. An injection seeded, Q-switched Nd:YAG laser operating at 532 nm with about 1000 mJ/pulse was used as the excitation laser source. The laser pulse width at FWHM was measured to be 8.4 ns. The injection seeding feature helps to produce a better pulse-to-pulse energy stability with less timing-jitter. Each pulse from the laser was temporally "stretched" to a longer pulse (75 ns halfwidth) by means of the pulse stretching optics [12] with 83 % energy throughput. The "pulse-stretcher" consists of sixteen mirrors and three beamsplitter-combiners. The beamsplitters divert fractions of the laser pulse to an optical delay line and subsequently recombine the multiple delayed pulses to a single, longer pulse. The pulse stretcher reduces the *peak* power to approximately 10 % of the input peak power as shown

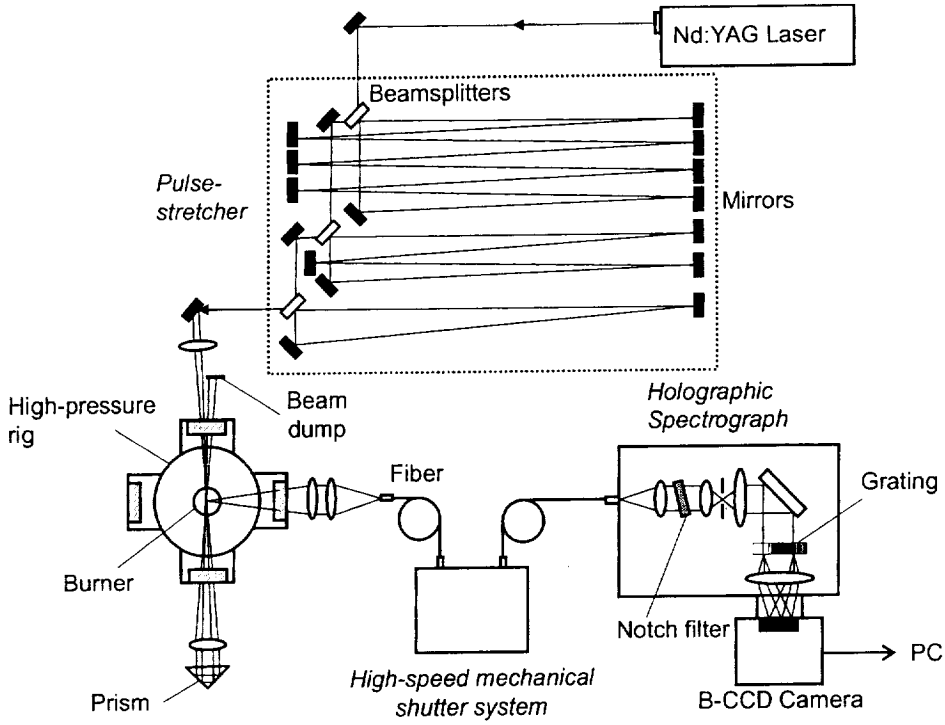

Fig.3 Schematic of Raman apparatus. Lasers, shutter, and camera are synchronized and controlled by a digital delay/pulse generation.

in Fig. 4 so that the laser pulse can be focused into the fine volume without the breakdown of gases as well as without damaging windows. Note that the breakdown of the air at high-pressure circumstances can be more significant because breakdown power threshold for the air has negative pressure dependence [27]. Using a 750 mm focal length lens, the light emerging from pulse stretcher was focused to a approximately 1 mm beam waist at the probe volume. The beam, after passing through the probe volume, was then reflected back into the probe volume using a 400 mm collimating lens and a right-angle prism; this effectively doubled the laser energy in the probe volume.

The vertically polarized Raman scattering light was collected at a 90-degree angle with a camera lens (85 mm, f/1.4) and was then focused onto a single silica optical fiber (400 μm in core diameter) connected to a electro-mechanical high-speed shutter [16] for gating the light. The proprietary shutter system design is based on electronically synchronized optical choppers. Figure 5 shows the optical transmission through the shutter system, which provided 24 μs exposure (FWHM) with 0.4 μs jitter with 12 x 0.4 mm clear aperture to reduce the effects of background light interferences. The gated light from the shutter was directed to the spectrograph. The optical throughput of the shutter system was 55 % including fiber transmission losses. The axially transmissive spectrograph (f/1.8) is fitted with a holographic notch filter to attenuate the Rayleigh scattering component of the signal by over six orders of magnitude. A volume holographic transmission grating disperses the signal into different wavelengths which are detected by a non-intensified, thermo-electrically cooled (-45 °C), back-illuminated CCD camera (1340 x 400 pixels) which provides approximately a 90 % quantum efficiency with 16-bits of dynamic range. The electronic exposure of the CCD was 5 ms (but the actual time exposure limited by the shutter is 24 μs), and the data was binned over 50 vertical pixels and accumulated for 250 shots (on the chip) to increase the signal-to-noise. The Spectral resolution was 0.31 nm for the 25 μm slit used. The spectral intensity was corrected to irradiance units ($W/cm^2/nm$) by means of the calibration of CCD count with calibration blackbody lamp so that it could be compared with theoretically calculated Raman spectra.

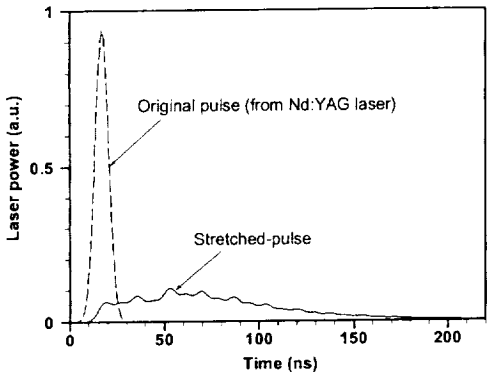

Fig. 4 Temporal profile of excitation laser pulse

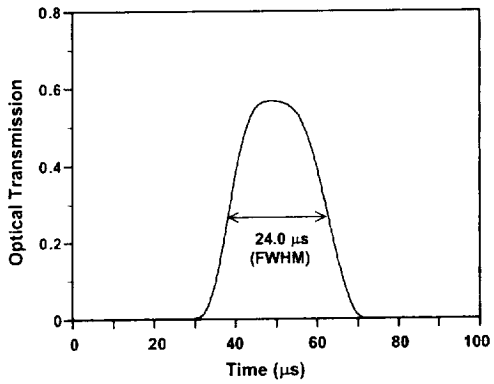

Fig. 5 Optical transmission through electro-mechanical shutter system. 250-shot averaged.

4. Results and Discussion

Laser Raman scattering measurements in combustion environments often suffer from background interferences such as flame luminosity and/or laser induced fluorescence of radicals. Removing these interferences is the key to a quantitative analysis. Here we have a steady flow and used a simple means for background subtraction. Figure 6 shows measured Raman spectra of rich H_2/air combustion gases at 20 atm. Even though Raman scattering was measured using a pulsed laser with a high-speed shutter system (24 μs exposure) to minimize spontaneous flame emissions and luminosity, a certain level of background was observed in the Raman scattering spectra as shown in Fig. 6(a). To remove this, the flame luminosity was measured without laser excitation and was subtracted from the original signal as shown in Fig.6(b). The pure Raman spectra then appeared as shown in Fig. 6(c). Rotational Stokes H_2 (rot-H_2), ro-vibrational Stokes of N_2 (vib-N_2), H_2O (vib-H_2O), and H_2 (vib-H_2) were observed clearly as well as anti-Stokes rotational H_2, and anti-Stokes ro-vibrational N_2. Very weak anti-Stokes vib-H_2 and H_2O were also observed. There are a couple of good candidates to determine the temperature in the present high-pressure flame: 1) Stokes rot-H_2; 2) Stokes vib-H_2; 3) Stokes/anti-Stokes vib-N_2. Stokes rot-H_2 Raman has stronger intensity in H_2 rich flames and each rotational spectrum is discriminated very well. Therefore we used the rot-H_2 spectra to estimate a temperature.

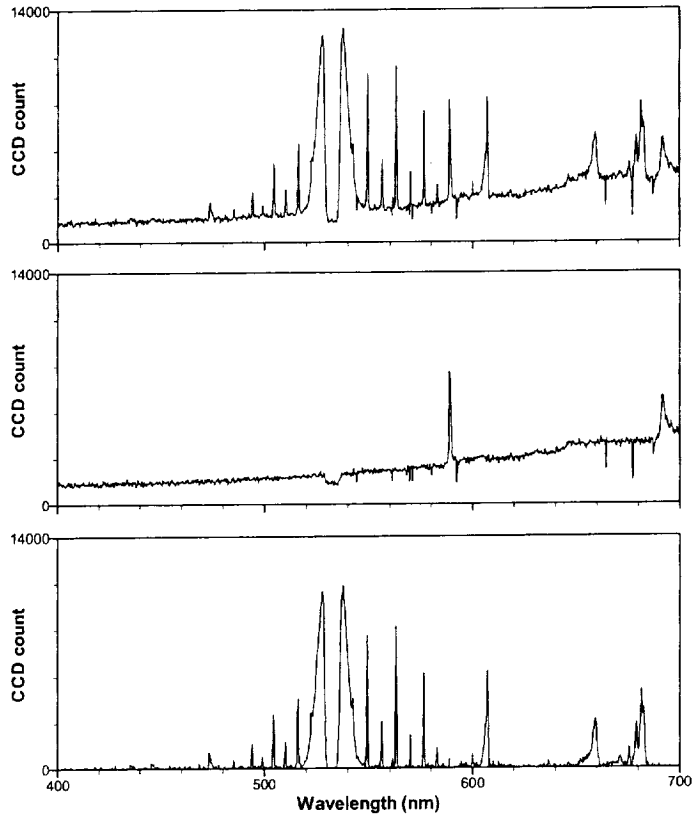

Fig. 6 Raman spectrum data in H_2/air combustion gases (ϕ = 1.34, 20atm, 250-shot). (a) laser Raman scattering with background flame luminescence, (b) flame luminescence without laser incident, (c) laser Raman scattering subtracted flame luminescence, that is (c) = (a) - (b). *a.s.* indicates anti-Stokes band, and *rot-* indicates pure rotational scattering. The profiles of Stokes and anti-Stokes rot-N_2 around 532 nm could be altered by the Notch filter. Spectral intensity is not calibrated to irradiance units. (a) and (b) were not measured simultaneously but used the same exposure time and accumulation number.

S-branches of rot-H_2 Raman spectra (close-up of Fig. 6) are shown in Fig. 7. Since S(0) and S(1) spectra tend to be overwhelmed by much stronger rot-N_2 signal unless some sort of polarization detection technique [8] is applied, relatively stronger signal from S(3) and S(5) could be good markers for temperature dependence of rot-H_2. Based on the theoretical model described above the integrated intensity ratio, R of S(3) to S(5) can be written as a function of T:

$$R(T) = \frac{f(3)}{f(5)} \exp\left(\frac{-hc(F(3) - F(5))}{kT} \right) \qquad (12)$$

where

$$f(J) = (2J+1) b_{J+2,J} (\nu_0 - \nu_k(J))^4 \qquad (13)$$

Substituting the experimental result of R in Fig. 7 for Eq.(12) the estimated temperature of 1889 K was determined. The theoretical rot-H_2 Raman spectrum at 1889 K and 20 atm was fitted to the experimental spectra as shown in Fig. 7. The experimental profile agrees well with that calculated for S-branches from J = 2 to 8 except J = 7. Since each rot-H_2 Raman between S(2) and S(6) is discriminated against each other due to relatively large rotational level spacing, and also because they do not suffer from any significant interferences, the profile of the spectrum can be a good place to examine pressure broadening effects. In the present experiment, however, the spectral resolution is much larger than the estimated pressure broadening, therefore the observed good agreement on the Raman spectral width between measured data and calculated as seen in Fig. 7 does not immediately support the pressure broadening coefficients assumed in the model.

The theoretical vib-H_2 Raman spectra at 1889 K and 20 atm was fitted to the experimental spectrum as shown in Fig. 8. Five major peaks in vib-H_2 agree well while the peaks at 676.7 nm and at 679.0 nm are slightly off. Such comparison between rotational temperature and vibrational temperature is a good way to evaluate the equilibrium condition. Figure 9 shows experimental vib-N_2 Raman spectra with theoretical

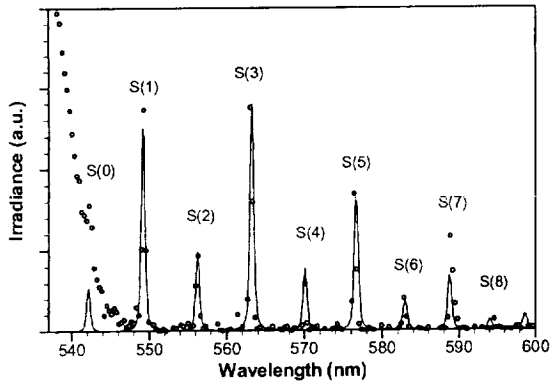

Fig. 7 Pure rotational Raman spectra of H_2 at 20 atm. *Dot* is experiment, *Line* is theoretical fit ($\Delta\nu_{spec}$ = 0.4 nm) at 1889 K. ϕ = 1.34 (H_2/air flame), 250-shot. A big difference between measured intensity and theoretical intensity in S(7) results from background subtraction error due to strong Na emission (shown in Fig. 7c) at that wavelength.

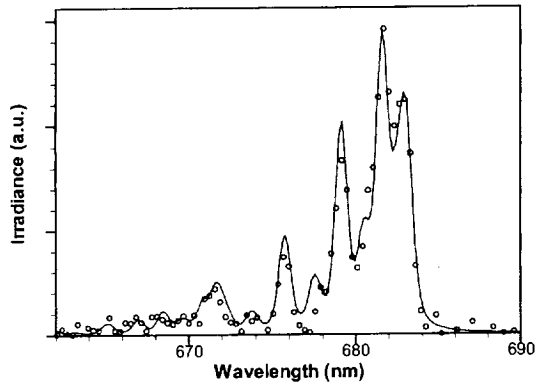

Fig. 8 Ro-vibrational H_2 Raman spectra at 20 atm. *Dot* is experiment, *Line* is theoretical fit ($\Delta\nu_{spec}$ = 0.4 nm) at 1889 K. ϕ = 1.34 (H_2/air flame), 250-shot.

fitting at 1889 K and 20 atm. The profiles all agree well in the three major vibrational transitions, so the estimated temperature is likely a reasonable equilibrium temperature.

5. Conclusions

A new high-pressure gaseous burner facility and a high-performance spontaneous Raman scattering diagnostics system (Nd-YAG based) have been developed to provide a fundamental, comprehensive Raman scattering spectral database in high-pressure flames for use as a quantitative calibration standard. These facilities were shown to provide high-quality Raman data with good signal-to-noise and sufficient spectral resolution. As the first demonstration, the Raman spectrum of H_2-Air combustion gases at 20 atm

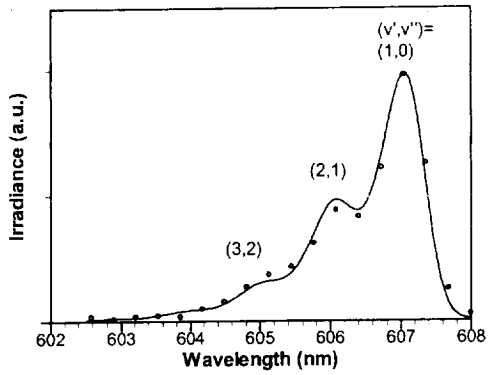

Fig. 9 Vibrational N_2 Raman spectra at 20 atm. *Dot* is experiment, *Line* is theoretical fit ($\Delta\nu_{spec}$ = 0.4 nm) at 1889 K. ϕ = 1.34 (H_2/air flame), 250-shot.

was measured. The theoretical spectra of pure rotational H_2 Raman and for vibrational H_2 Raman were calculated using a classical harmonic-oscillator model and a line-shape model including pressure broadening and were compared to the experimental data to estimate the temperature. The clear rotational and ro-vibrational Raman spectra of H_2, N_2, H_2O were observed after subtraction of flame luminescence and radiations. Theoretical spectral analysis on experimental rot-H_2 Raman provided an estimated gas temperature of 1889 K in H_2-Air combustion at ϕ = 1.34, 20 atm. Calculated Raman spectra of rot-H_2, vib-H_2, and vib-N_2 agreed well with the experimental results. This result indicates that the estimated spectroscopic temperature obtained from H_2 seems to be a reasonable value, however the temperature measured here should be evaluated by other methods e.g. Rayleigh thermometry or chemical equilibrium computation. Also this H_2 Raman thermometry will be competed with N_2 Raman thermometry in high-pressure environments. More detailed quantitative spectral analysis of high-pressure Raman spectra in various flame conditions will be done by means of theoretical computation, and additional more precise experimental data are needed.

This work was supported principally by the Ultra-Efficient Engine Technologies (UEET) Program, and by the Zero CO_2 Emissions Technologies (ZCET) Program at NASA Glenn Research Center. This work was performed while the author held a National Research Council Research Associateship Award at NASA Glenn Research Center. The authors acknowledge Mr. Gregg Calhoun, Mr. William Pryfogle, Mr. William Thompson, Mr. Raymond Lotenero, Mr. Gary Lorenz, and Ms. Paulette Adams for their assistance in the construction and operation of the facilities.

References

1. A. C. Eckbreth, *Laser Diagnostics for Combustion Temperature and Species*: 2nd Ed., Gordon and Breach Publishers, The Netherlands, 209-273, (1996).
2. E. W. Roths, and P. Andresen, "Application of Tunable Excimer lasers to Combustion Diagnostics: a Review," *Appl. Opt.* **36**:18, 3971-4033, (1997).
3. G. Zikratov, F.-Y. Yueh, J. P. Singh, O. P. Norton, R. A. Kumar, and R. L. Cook, "Spontaneous Anti-Stokes Raman probe for Gas Temperature Measurements in Industrial Furnaces," *Appl. Opt.* **38**:9, 1467-1475, (1999).
4. T. A. Berkoff, D. N. Whiteman, R. D. Rallison, G. K. Schwemmer, L. Ramos-Izquierdo, and H. Plotkin, "Remote Detection of Raman Scattering by Use of a Holographic Optical Element as a Dispersive Telescope," *Opt. Lett.* **25**:16, 1201-1203, (2000).
5. R. Locke, Y. Hicks, W. De Groot, and R. Anderson, "Spontaneous Raman Scattering: from Atmospheric CH_4/air Diffusion Flame to 55 Bar Jet-A-Fueled, Aviation Gas Turbine Combustor," 22nd AIAA Aerodynamic Measurement Technology: Ground Testing Conference, St. Louis, AIAA Paper No. 2002-3040, (2002).
6. E. P. Hassel, "Ultraviolet Raman-Scattering Measurements in Flames by the Use of a Narrow-Band XeCl Excimer Laser," *Appl. Opt.* **32**:21, 4058-4065, (1993).
7. M. S. Mansour, and Y.-C. Chen, "Line-Raman, Rayleigh, and Laser-Induced Predissociation Fluorescence Technique for Combustion with a Tunable KrF Excimer Laser," *Appl. Opt.* **35**:21, 4252-4260, (1996).
8. Y. Gu, E. W. Rothe, and G. P. Reck, "One-Dimensional Imaging of H_2 Densities and of Temperatures via Rotational Raman Scattering of Narrow-Band, 248 nm, Laser Light," *J. Raman Spectrosc.* **28**, 605-612, (1997).
9. F. Rabenstein, and A. Leipertz, "One-Dimensional, Time-Resolved Raman Measurements in a Sooting Flame Made with 355-nm Excitation," *Appl. Opt.* **37**:21, 4937-4943, (1998).
10. M. Decker, A. Schik, U. E. Meier, and W. Stricker, "Quantitative Raman Imaging Investigations of Mixing Phenomena in High-Pressure Cryogenic Jets," *Appl. Opt.* **37**:24, 5620-5627, (1998).
11. Q. V. Nguyen, R. W. Dibble, C. D. Carter, G. J. Fiechtner and R. S. Barlow, "Raman-LIF Measurements of Temperature, Major Species, OH, and NO in a Methane-Air Bunsen Flame," *Comb. Flame* **105**, 499-510, (1996).
12. J. Kojima, and Q. V. Nguyen, "Laser Pulse-Stretching Using Multiple Optical Ring-Cavities," *Appl. Opt.*, submitted.
13. M. Gittins, S. U. Shenoy, H. R. Aldag, D. P. Pacheco, M. F. Miller, and M. G. Allen, "Measurements of Major Species in a High Pressure Gas Turbine Combustion Simulator Using Raman Scattering," 38th AIAA Aerospace Science Meeting & Exhibit, Reno, AIAA Paper No. 2000-0772, (2000).
14. P. C. Miles, "Raman Line Imaging for Spatially and Temporally Resolved Mole Fraction Measurements in Internal Combustion Engines," *Appl. Opt.* **38**:9, 1714-1732, (1999).
15. R. S. Barlow, and P. C. Miles, "A Shutter-Based Line-Imaging System for Single-Shot Raman Scattering Measurements of Gradients in Mixture Fraction," *Proc. Combust. Inst.* **28**, 269-277, (2000).
16. Q. V. Nguyen, "High Speed Electromechanical Shutter for Imaging Spectrographs," NASA Disclosure of New Invention and Technology, LEW17, 175-1, (2001).
17. M. Knapp, A. Luczak, V. Beushausen, W. Hentschel, P. Manz, and P. Andresen, "Polarization Separated Spatially Resolved Single Laser Shot Multispecies Analysis in the Combustion Chamber of a Realistic SI Engine with a Tunable KrF Excimer Laser," *Proc. Combust. Inst.* **26**, 2589-2596, (1996).
18. Y. Gu, Y. Zhou, H. Tang, E. W. Rothe, and G. P. Reck, "Presure Dependence of Vibrational Raman Scattering of Narrow-Band, 248-nm, Laser Light by H_2, N_2, O_2, CO_2, CH_4, C_2H_6, and C_3H_8 as High as 97 bar," *Appl. Phys. B* **71**, 865-871, (2000).
19. D. A. Long, *Raman Spectroscopy*, McGraw-Hill, London, (1977).
20. G. Hertzberg, *Molecular Spectra and Molecular Structure - I. Spectra of Diatomic Molecules*: 2nd Ed., Krieger Publishing Company, Florida, (1950).
21. K. P. Huber, and G. Hertzberg, *Molecular Spectra and Molecular Structure - IV. Constants of Diatomic Molecules*, Van Nostrand Reinhold Company, New York, (1979).
22. S. R. Drayson, "Rapid Computation of the Voigt Profile," *J. Quant. Spectrosc. Radiat. Transfer* **16**, 611-614, (1976).
23. A. P. Thorne, *Spectrophysics*, Chapman and Hall, London, (1974).
24. L. S. Rothman, C. P. Rinsland, A. Goldman, S. T. Massie, D. P. Edwards, J.-M. Flaud, A. Perrin, C. Camy-Peyret, V. Dana, J.-Y. Mandin, J. Schroeder, A. McCann, R. R. Gamache, R. B. Wattson, K. Yoshino, K. V. Chance, K.W. Jucks, L.R. Brown, V. Nemtchinov, and P. Varanasi, "The HITRAN Molecular Spectroscopic Database and HAWKS (HITRAN Atmospheric Workstation): 1996 Edition," *J. Quant. Spectrosc. Radiat. Transfer* **60**, 665-710, (1998).
25. A. Lévy, N. Lacome, and C. Chackerian, "Collisional Line Mixing": in *Spectroscopy of the Earth's Atmosphere and Interstellar Medium*, Academic Press, San Diego, 261-422, (1992); and references therein.
26. K. L. McNesby, and J. B. Morris, "Fourier Transform Raman Spectroscopy of Nitrogen at High Pressure," *J. Raman Spectrosc.* **26**, 487-490, (1995).
27. T. X. Phuoc, "Laser Spark Ignition: Experimental Determination of Laser-Induced Breakdown Thresholds of Combustion Gases," *Opics. Communications* **175**, 419-423, (2000).